In-situ transmission electron microscopy investigation of the deformation mechanism in CoCrNi and $CoCrNiSi_{0.3}$ nanopillars

Cheng-Ling Tai [a], Jhen-De You [a], Jia-Jun Chen [a], Shu-Cheng Liang [a], Tsai-Fu Chung [b], Yo-Lun Yang [c], Seiichiro Ii [d], Takahito Ohmura [d], Xiao-Yang Zheng [e], Chih-Yuan Chen[f], Jer-Ren Yang [a,*]

[a] Department of Materials Science and Engineering, National Taiwan University, Taipei 10617, Taiwan.

[b] Department of Materials Science and Engineering, National Yang Ming Chiao Tung University, Hsinchu, Taiwan.

[c] Department of Mechanical Engineering, National Taipei University of Technology, Taipei, Taiwan.

[d] National Institute for Materials Science, 1-2-1 Sengen, Tsukuba, Ibaraki 305-0047, Japan

[e] Department of Mechanical Engineering, Graduate School of Engineering, The University of Tokyo, Tokyo, Japan

[f] Graduate Institute of Intellectual Property, National Taipei University of Technology, Taipei, Taiwan

*Corresponding author: Jer-Ren Yang

Tel: +886–2–33661314

Fax: +886–2–23634562

E-mail of Corresponding author: jryang@ntu.edu.tw

Graphical Abstract

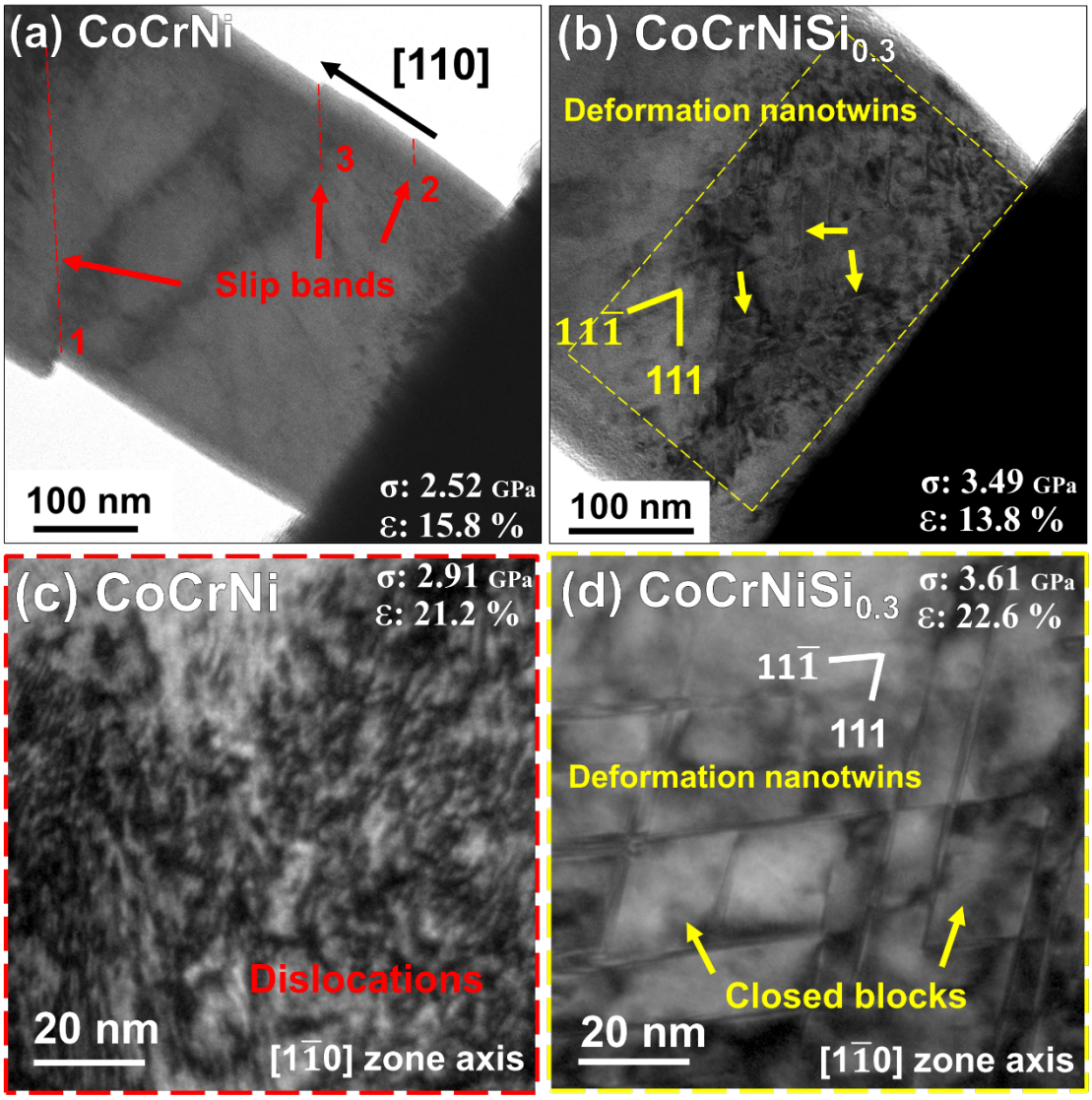

Highlights:

1. Compression tests with a constant strain rate of 2×10^{-3} s^{-1} on CoCrNi and $CoCrNiSi_{0.3}$ nanopillars in a transmission electron microscope have been investigated.
2. In the CoCrNi nanopillar, slip bands rather than deformation twins formed during compression along [110].
3. The first strain burst in the $CoCrNiSi_{0.3}$ nanopillar occurred later than that in CoCrNi, with 39 % higher strength.
4. The formation of deformation nanotwins in the $CoCrNiSi_{0.3}$ nanopillar inhibited the formation of slip-bands.

Abstract

CoCrNi and $CoCrNiSi_{0.3}$ nanopillars exhibited distinct deformation behaviors under in-situ compression experiments with a strain rate of 2×10^{-3} s^{-1} in a transmission electron microscope. The former was mainly deformed through slip-dislocations and the formation of slip-bands with edges extending to the nanopillar's boundaries; in contrast, the latter was primarily deformed by twinning and partitioned by deformation nanotwins, with different variants intersecting each other to form closed nano-blocks. Si addition not only enhanced the solid solution strengthening effect but also facilitated the formation of nanotwins, resulting in a delayed first strain burst in the $CoCrNiSi_{0.3}$ nanopillar at a strain of 9.6 % with strength 39 % higher than that in CoCrNi at a strain of 7.1 % during the in-situ deformation. In addition, closed nano-blocks effectively strengthened the $CoCrNiSi_{0.3}$ nanopillar, which possessed strength 24 % higher than that of the CoCrNi nanopillar at the same strain of ~20 %.

Keywords: In-situ compression transmission electron microscopy; CoCrNi nanopillar; Silicon addition; Deformation nanotwins; Dislocations

In recent years, single-phase FCC-type high entropy alloys (HEAs) have been innovated [1, 2], and rapid advancements have followed due to their exceptional attributes, including their corrosion resistance [3] and mechanical properties [4-7]. Extensive research [4-12] has been dedicated to HEAs, which overcome the trade-off dilemma between strength and ductility in common materials. During deformation, the low stacking fault energy (SFE) in CoCrFeMnNi HEAs, in the range of only 20–30 mJm^{-2} [10, 13], facilitates the formation of deformation twins during plastic deformation, leading to simultaneous enhancements in both strength and ductility, particularly at cryogenic temperatures [5, 7] and high strain rates [6].

Moreover, FCC-type CoCrNi medium entropy alloys (MEAs), with a stacking fault of 17.4 mJm^{-2} [14], have garnered considerable attention owing to their superior mechanical properties [15-17]. Equal-molar HEAs exhibit mixing entropy values greater than 1.61R (13.38 J/K·mol, where R is the gas constant, 8.314 J/K·mol), while MEAs fall within the range of 0.69R to 1.61R [18]. A previous work [19] claimed that CoCrNi MEAs possessed nearly the same critical twinning stress as that of CoCrFeMnNi HEAs, but the earlier formation of deformation twins in the former (ε = 13 % with σ = 1230 MPa) led to the higher UTS than that of the latter (ε = 20 % with σ = 870 MPa). Nonetheless, a weakness of FCC-type HEAs and MEAs is their low strength at room temperature. To address this limitation, various minor elements, both metallic (e.g., Al [8], V [9]) and non-metallic (e.g., C [11], Si [12, 14, 20], B

[21], N [22]), have been incorporated into FCC-type HEAs and MEAs to enhance their mechanical strength.

Prior works indicated that a suitable addition of Si to CoCrFeMnNi HEAs [12, 23] and CoCrNi MEAs [14, 20, 24, 25] could significantly enhance their overall mechanical properties. The improvement was attributed not only to solid solution strengthening but also to the reduction of the stacking fault energy resulting from Si addition [12, 14, 23]. A previous investigation [12] on $CoCrFeMnNiSi_x$, (x denoted the content of 1-5 at. %) HEAs claimed that the Si content was a critical factor in the alloys' strength and deformation mechanism. It was claimed [12] that CoCrFeMnNi HEAs with a higher Si content (5 at. %) mainly deformed through dislocation movement, while those with a lower Si content (1 - 4 at. %) exhibited deformation twinning. However, in ternary CrCoNi MEAs, a previous work [14] reported that the ultimate tensile strength (UTS) of $CrCoNiSi_{0.3}$ MEA (an addition of 9.1 at. % Si) was 22 % higher than that of CrCoNi MEA, primarily due to the lower SFE (4.7 mJm^{-2}) in the former alloy, which facilitated the formation of nanotwins and a hexagonal close-packed (HCP) structure during deformation. Another work [20] on CrCoNi MEA also confirmed that the ultimate tensile strength of $CrCoNiSi_{0.2}$ MEA was 16 % higher than that of the equiatomic CrCoNi MEA. In addition, the $CrCoNiSi_{0.3}$ MEA compressed at different strain rates has also been investigated [25]. A higher strain rate led to the earlier occurrence of deformation twins, with a true strain of 16 % at the high compression rate (6×10^3 s^{-1}) but that of 30 % at the low

one (10^{-3} s^{-1}). Although the above works claimed the benefits of Si addition, the deformation in the alloys was investigated only in ex-situ experiments, which might not have allowed observation of more details of the corresponding defect structures correlated to the mechanical properties during the course of deformation.

Recently, a few in-situ deformation investigations of CoCrFeNiMn [26, 27] and $FeCoNiCrAl_{0.1}$ [28] were observed by transmission electron microscopy (TEM); however, the related evolution of defects during the course of deformation was not reported. The correlation of deformed structures with mechanical properties in small-sized applications such as micro-electro-mechanical systems has become an essential focus in recent years. In the present work, $CoCrNiSi_{0.3}$ and CoCrNi nanopillars were directly investigated by in-situ compression tests in a transmission electron microscope.

The equiatomic CoCrNi and $CoCrNiSi_{0.3}$ (molar ratio) MEAs employed in the present work were prepared via arc-melting using high-purity (> 99.9 wt. %) metals. To eliminate dendrite formation during the casting process, both samples were homogenized at 1100 °C for 2 days in a vacuum furnace, followed by cold rolling with a 70 % thickness reduction and annealing treatment at 1100 °C for 2 h to attain an optimal grain size. Subsequently, the samples were abraded with 800# to 4000# SiC sandpaper and twin-jet polished at 25 V using a mixture of 5% $HClO_4$ and 95% CH_3COOH to eliminate scratches and strains on the sample surfaces. For the compression direction in the in-situ TEM experiments, the 110 pole of the specimen

was determined by electron backscatter diffraction (EBSD) in a scanning electron microscope (SEM, FEI Nova NanoSEM 450), as illustrated in Supplementary Fig. 1a of Supplementary Material I. The selected area was then processed with a focused ion beam (FIB, FEI Helios 600i) to extract a 20 μm × 20 μm × 1 μm thin plate, which was affixed to a mesh through Pt deposition (Supplementary Fig. 1b of Supplementary Material I). Subsequently, nanopillars measuring 300 nm in width, 600 nm in length, and approximately 100 nm in thickness were shaped by FIB (Supplementary Fig. 1c of Supplementary Material I). In-situ compression tests and observations (Supplementary Fig. 1d of Supplementary Material I) were conducted in a transmission electron microscope (TEM, JEOL ARM300F) equipped with a Hysitron PicoIndenter. The larger magnification was chosen during the in-situ tests to ensure the detection of the formation of deformation nanotwins. These experiments were performed under the two-beam condition, with the g = [1 1 0] orientation (Supplementary Fig. 1e of Supplementary Material I), and the compression tests employed a constant strain rate of approximately 2×10^{-3} s^{-1}. The chemical compositions of CoCrNi and $CoCrNiSi_{0.3}$ nanopillars were analyzed using Energy-Dispersive X-ray Spectroscopy (EDS) mapping in the TEM and were found to be nearly identical to those of the bulk materials.

Figs. 1a and b respectively present the initial TEM images of the CoCrNi and $CoCrNiSi_{0.3}$ nanopillars before deformation. After annealing at 1100 °C for 2 h, both nanopillars displayed a single crystal structure, without the presence of annealing nanotwins. The nanopillars were

consistently deformed by nano-indenter from the lower right corner toward the upper left corner, along the [110] direction.

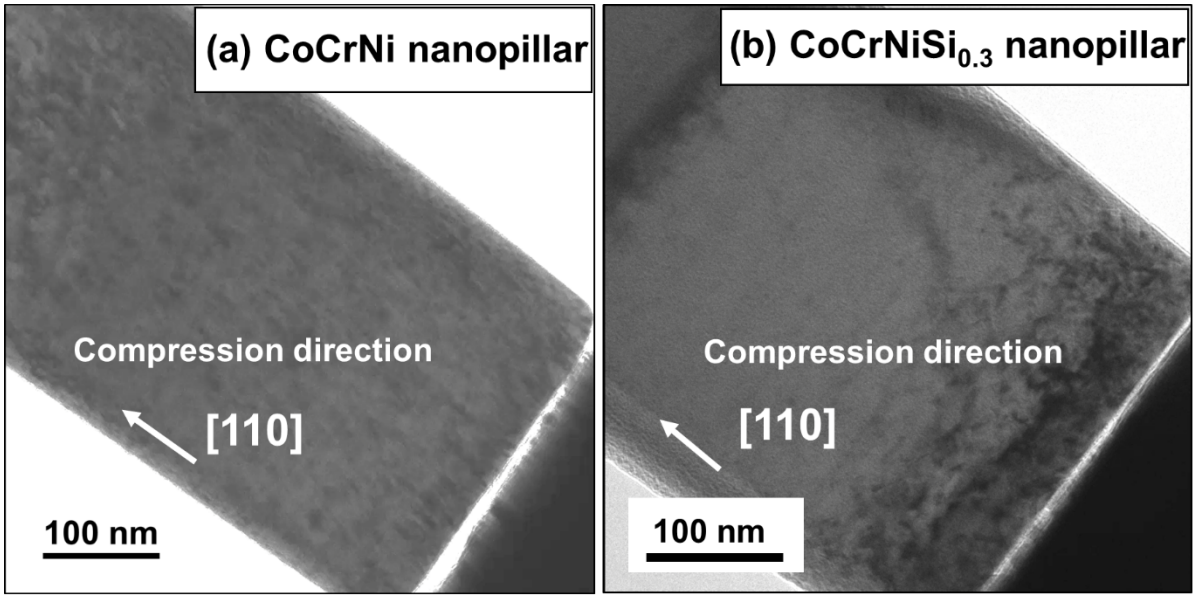

Fig. 1. TEM images of the (a) CoCrNi and (b) $CoCrNiSi_{0.3}$ nanopillars prior to deformation.

Fig. 2a shows the stress–strain curve obtained from the execution load divided by the contact area on the CoCrNi nanopillars. Figs. 2 b-f illustrate the image frames captured from Video 1 (provided in Supplementary Material II), recording the in-situ compression test conducted on the CoCrNi nanopillar. As the chosen compression direction was [110], four of the twelve slip systems, $<0\bar{1}1>/\{111\}$, were presumably activated. The reduction in activated slip systems made it more difficult to achieve the critical shear stress required for twining. In addition, under TEM observation of the $[1\bar{1}0]$ zone axis, two slip planes, $(11\bar{1})$ and (111), are in edge-on configuration, which facilitates to estimate the thickness of deformation nanotwins and further explore their development in CoCrNi and $CoCrNiSi_{0.3}$ nanopillars during

compressive deformation. Following elastic deformation, as depicted in Fig. 2a, the strength reached 2.26 GPa (with ε = 7.1 %), followed by the first strain burst at 1.97 GPa (with ε = 7.3 %). It is important to note that the pop-in event was caused by the escape of dislocations and does not signify a weakening of the sample. Previous works on nanopillars of BCC steels in a TEM [29, 30] activated eight of the $\{0\bar{1}1\}/\langle 111\rangle$, $\{\bar{2}11\}/\langle 111\rangle$, and $\{\bar{3}21\}/\langle 111\rangle$ slip systems [31]. The strain burst here occurred due to the escape of a substantial number of dislocations, which moved to the surfaces of the nanopillars, known as dislocation avalanches [32, 33]. In contrast to the BCC structure, the present work on the FCC structure, which activated four of the twelve slip systems on the {111} plane, showed that the first two slip bands formed and extended beyond the two side boundaries (denoted as Slip bands 1 and 2 in Fig. 2b) This sudden reduction in the pillar's length resulted in a gap between the specimen and the indenter, leading to the stress relaxation. In addition, the forming process might have induced lateral diffusion of Ga damage, potentially reducing the thickness at the top of the pillar, leading to a slightly smaller contact area than the rest of the pillar, and resulting in a lower calculated Young's modulus. In current work, this phenomenon is difficult to avoid.

As the deformation continued, the strength increased and then experienced a slight decrease to 2.20 GPa at 8.9 % strain, resulting from the formation of an extended step in the left side of the pillar (Slip band 1), as shown in Fig. 2c. As the deformation proceeded, the compression process further enhanced the strength to 2.60 GPa (Fig. 2a) due to the prevalence

of newly formed dislocations outweighing those escaping to the surface. Subsequently, a large number of dislocations suddenly disappeared while the step size of Slip band 1 increased beyond the pillar surface, creating substantial gaps between the specimen and the indenter and causing a significant strain burst at ε = 10.9 % until σ = 1.50 GPa, as depicted in Fig. 2d. As the load increased further, another strain burst took place at strain of 15.8 %, which was associated with the formation of the third slip band (Slip band 3) on the right side of the pillar (Fig. 2e). As the compression continued, a fluctuation in the stress–strain curve occurred (Fig. 2a), attributed to the escape of dislocations and the extension of a newly formed slip band (Slip band 4) beyond the specimen surface, as illustrated in Fig. 2f. The previous works on the bulk materials of CoCrNi MEAs [15-17] claimed that deformation twins could occur during the course of standard tensile deformation; however, only slip bands were observed on the CoCrNi nanopillar in the present work.

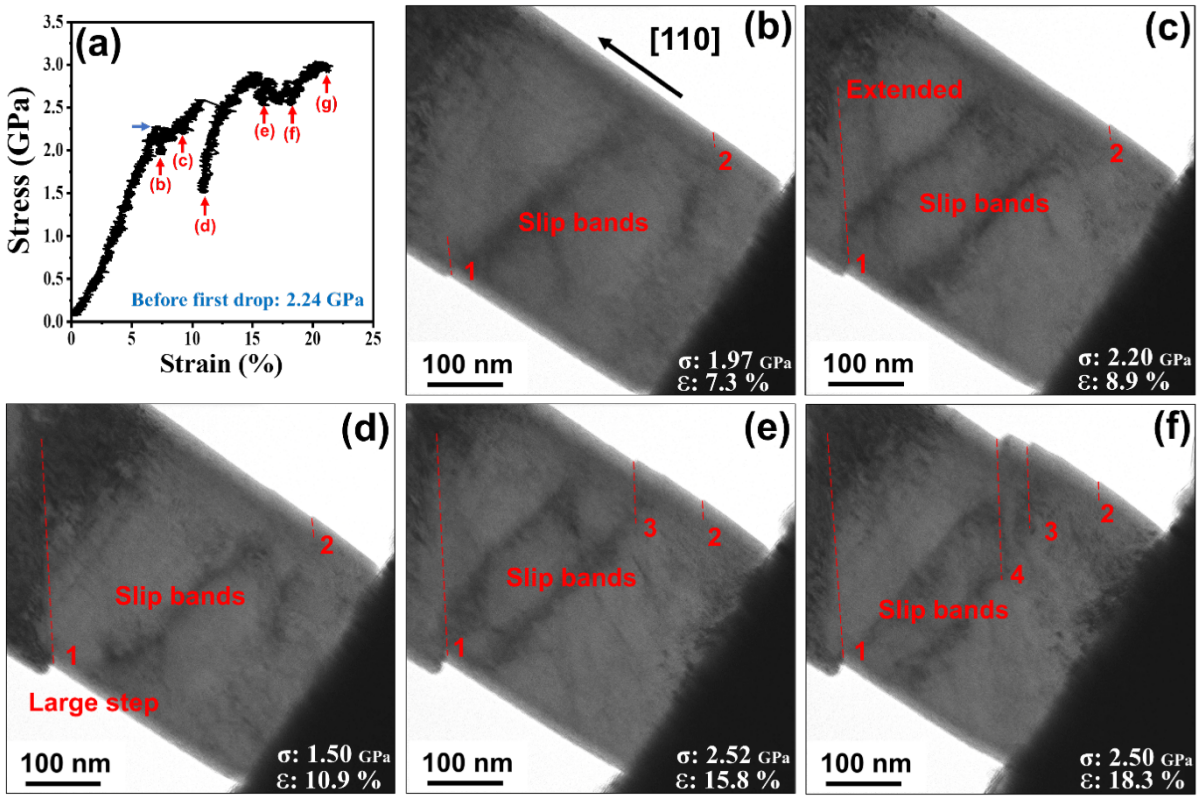

Fig. 2. CoCrNi nanopillar's (a) Stress–strain curve. TEM images of (b)-(f) strain burst with escape of dislocations and formation of slip bands in the nanopillar.

Fig. 3a presents the stress–strain curve of the $CoCrNiSi_{0.3}$ nanopillar. Figs. 3b-f display individual frames extracted from Supplementary Material III (Video 2), depicting the in-situ compression deformation of the $CoCrNiSi_{0.3}$ nanopillar. The critical strength for deformation twin occurrence in the $CoCrNiSi_{0.3}$ nanopillar was measured at 2.65 GPa (with $\varepsilon = 5.8$ %), as shown in Fig. 3b. Notably, despite the yielding point being exceeded, no obvious initial strain burst was observed in the $CoCrNiSi_{0.3}$ nanopillar. This phenomenon can presumedly be attributed to two factors. First, the addition of Si yielded a more effective solid solution strengthening effect in comparison to that of the CoCrNi nanopillar. This effect hindered the mobility of dislocations, thus suppressing the serration in the stress–strain curve. Secondly, the

Si addition in $CoCrNiSi_{0.3}$ MEA reduced the stacking fault energy [14], decreasing the critical shear stress required for activating Shockley partial dislocations. Instead of dislocations escaping to the surface, Shockley partials in the $CoCrNiSi_{0.3}$ nanopillar glided on (111) planes to form deformation twins [28] during the compression, preventing the strain burst at strength of 2.65 GPa (point b in Fig. 3a).

As the load progressed, more deformation twins formed on two slip planes, $(1\bar{1}1)$ and $(\bar{1}11)$, and efficiently impeded the movement of dislocations, leading to a higher strength of 3.11 GPa (with strain of 9.6 %), which was 39 % higher than that of the CoCrNi nanopillar. Suddenly, the first strain burst occurred in the $CoCrNiSi_{0.3}$ nanopillar at strain of 10.1 % (with strength of 2.86 GPa) because the dislocations avalanched at the position where deformation twins had yet to form (as indicated in Fig. 3c by the red arrow). As shown in Fig. 3d, densely distributed deformation twins throughout the $CoCrNiSi_{0.3}$ nanopillar, accompanied by a large number of dislocations (with dark contrast strain field), contributed to the strength increment (σ = 3.49 GPa with ε = 13.8 %). Subsequent to a small amount of strain, certain deformation twins and dislocations disappeared (Fig. 3e), causing a slight strain burst at σ = 3.02 GPa (with ε = 14.7 %). Following this decrement, a significant drop immediately occurred, leading to σ = 1.95 GPa (with ε = 17.0 %), as shown in Fig. 3a. Fig. 3f presents the corresponding TEM image elucidating that this huge strain burst can be attributed to the depletion of substantial deformation twins and dislocations. Interestingly, no slip bands were observed at the

boundaries, implying the presence of other sites for defects to be annihilated, as will be discussed in later paragraphs.

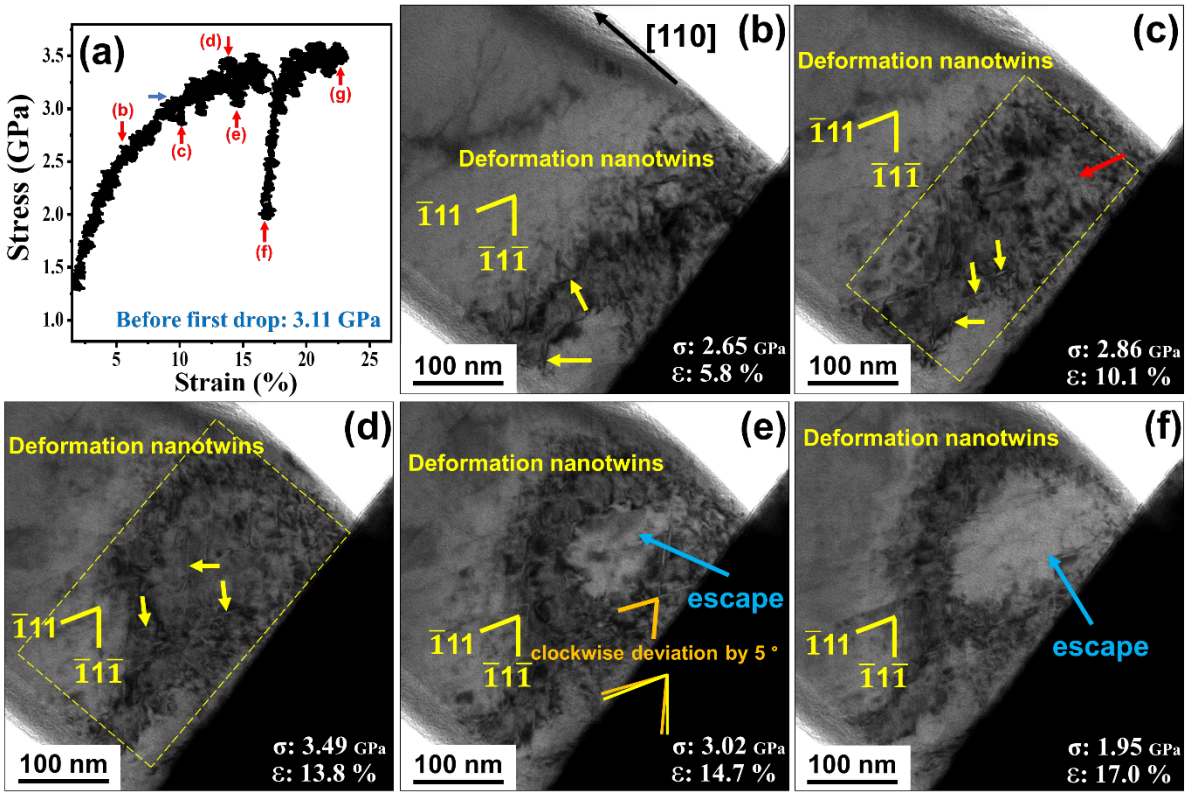

Fig. 3. CoCrNiSi0.3 nanopillar's (a) Stress–strain curve. TEM images of (b)-(d) deformation twins impeding dislocations, and (e) and (f) strain bursts with escape of deformation twins and dislocations in the nanopillar.

Figs. 4a and c respectively show TEM images of the CoCrNi and $CoCrNiSi_{0.3}$ nanopillars at the final stage, along with their corresponding magnified images under the $[1\bar{1}0]$ exact zone axis (Figs. 4b and d). Unlike the standard tensile tests performed on the CoCrNi alloy in previous works [15, 34], which revealed a twinning mechanism after a certain level of strain was reached, the slow compression test on nanopillars deformed along the [110] direction revealed that, instead of deformation twins, only dislocations were introduced into the CoCrNi nanopillar even when the strain reached 21.2 % (with σ = 2.91 GPa), as shown in Fig. 4b. The

corresponding diffraction pattern exhibited merely diffraction spots from the matrix. This result can probably be attributed to the chosen compression direction, [110], which activated only one third of the 12 slip systems in the FCC structure, resulting in a lack of dislocation accumulation to reach the critical shear stress for Shockley partial dislocations.

In contrast, the addition of Si to the CoCrNi nanopillar led to the immediate formation of deformation twins after the elastic deformation, as shown in Fig. 3b. This observation confirmed that the addition of Si indeed reduced the stacking fault energy, which was consistent with the theorical calculation results [14], leading to enhancement of the work hardening rate. The formation of deformation twins on two slip planes, $(\bar{1}11)$ and $(\bar{1}1\bar{1})$, efficiently hindered the movement of dislocations. Furthermore, following a certain level of deformation, a notable abundance of defects was observed in the $CoCrNiSi_{0.3}$ nanopillar. These saturated defects rendered the deformation process more challenging, forcing the pillar to deform in an easier way, i.e., distortion, as shown in Fig. 4c. Consequently, deformation twins and dislocations could escape from the nanopillar at the upper and lower surfaces through this distortion, as shown in Fig. 3e, marking the beginning of bending that caused the deformation twins to deviate each other (clockwise by 5° indicated by yellow and orange line as indicated in Fig. 3e). The distortion led to the formation of a bending contour, as shown in Fig. 4c, and thus no contribution to the increment in strength (Fig. 3a). The enlarged image from Fig. 4c shown in Fig. 4d shows that at the high strain level (ε = 22.6 % with σ = 3.61 GPa), deformation

nanotwins with an average thickness of 2.24 nm on (111) and (11$\bar{1}$) intersected and formed plenty of closed blocks of about 10-20 nanometer sizes which possessed a dynamic grain refinement effect [6].

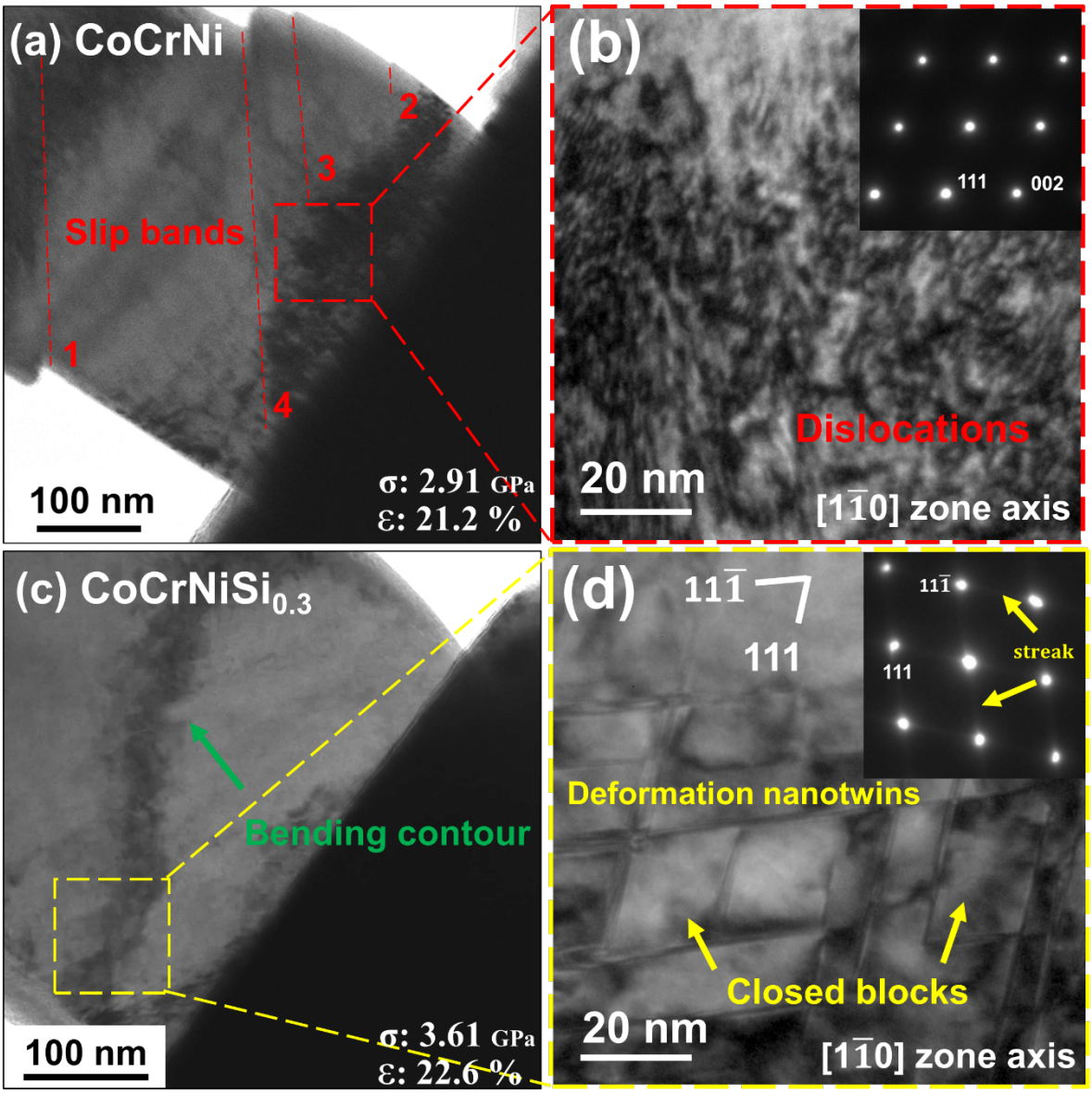

Fig. 4. (a) The final stage TEM image of the CoCrNi nanopillar with (b) the enlarged image from (a). (c) The final stage TEM image of the $CoCrNiSi_{0.3}$ nanopillar with (d) the enlarged image from (c).

In summary, in-situ compression tests were conducted under a transmission electron microscope to investigate the deformation behaviors of CoCrNi and $CoCrNiSi_{0.3}$ nanopillars.

The CoCrNi nanopillar primarily involved dislocation movement, leading to the formation of slip bands extending beyond the boundaries. This behavior was different from that of CoCrNi general tensile-test bulk samples, which deformed via deformation twins after undergoing a certain strain. The Si addition in the CoCrNi nanopillar not only contributed to the solid solution strengthening effect but also lowered the stacking fault energy, leading to easier formation of Shockley partial dislocations. The prevalence of partial dislocations contributed to higher strength and a delay in the first strain burst in the $CoCrNiSi_{0.3}$ nanopillar, the strength of which was 39 % higher than that of the CoCrNi nanopillar. In addition, deformation nanotwins formed closed blocks (with a size of about 20 nm x 20 nm) in the $CoCrNiSi_{0.3}$ nanopillar, interrupting dislocation movement and preventing the escape of dislocations to the nanopillar's boundaries. The $CoCrNiSi_{0.3}$ nanopillar is more stable during the compressive deformation, and can be suggested for tiny-sized applications.

Acknowledgments: This work received financial support from the Japan–Taiwan Exchange Association and the National Science and Technology Council, Taiwan, under contract NSTC-112-2224-E-002-004.

References

[1] J.W. Yeh, S.K. Chen, S.J. Lin, J.Y. Gan, T.S. Chin, T.T. Shun, C.H. Tsau, S.Y. Chang,

Nanostructured high-entropy alloys with multiple principal elements: novel alloy design concepts and outcomes, Advanced engineering materials 6(5) (2004) 299-303.

[2] B. Cantor, I. Chang, P. Knight, A. Vincent, Microstructural development in equiatomic multicomponent alloys, Materials Science and Engineering: A 375 (2004) 213-218.

[3] Y. Chen, T. Duval, U. Hung, J. Yeh, H. Shih, Microstructure and electrochemical properties of high entropy alloys—a comparison with type-304 stainless steel, Corrosion science 47(9) (2005) 2257-2279.

[4] Y. Zhang, T.T. Zuo, Z. Tang, M.C. Gao, K.A. Dahmen, P.K. Liaw, Z.P. Lu, Microstructures and properties of high-entropy alloys, Progress in materials science 61 (2014) 1-93.

[5] G. Laplanche, A. Kostka, O. Horst, G. Eggeler, E. George, Microstructure evolution and critical stress for twinning in the CrMnFeCoNi high-entropy alloy, Acta Materialia 118 (2016) 152-163.

[6] T.-F. Chung, P.-J. Chen, C.-L. Tai, P.-H. Chiu, Y.-S. Lin, C.-N. Hsiao, C.-Y. Chen, S.-H. Wang, J.-W. Yeh, W.-S. Lee, Investigation of nanotwins in the bimodal-structured Fe22Co22Ni20Cr22Mn14 alloy subjected to high-strain-rate deformation at cryogenic temperatures, Materials Characterization 170 (2020) 110667.

[7] B. Gludovatz, A. Hohenwarter, D. Catoor, E.H. Chang, E.P. George, R.O. Ritchie, A fracture-resistant high-entropy alloy for cryogenic applications, Science 345(6201) (2014)

1153-1158.

[8] J. He, W. Liu, H. Wang, Y. Wu, X. Liu, T. Nieh, Z. Lu, Effects of Al addition on structural evolution and tensile properties of the FeCoNiCrMn high-entropy alloy system, Acta Materialia 62 (2014) 105-113.

[9] B. Yin, F. Maresca, W. Curtin, Vanadium is an optimal element for strengthening in both fcc and bcc high-entropy alloys, Acta Materialia 188 (2020) 486-491.

[10] N.L. Okamoto, S. Fujimoto, Y. Kambara, M. Kawamura, Z.M. Chen, H. Matsunoshita, K. Tanaka, H. Inui, E.P. George, Size effect, critical resolved shear stress, stacking fault energy, and solid solution strengthening in the CrMnFeCoNi high-entropy alloy, Scientific reports 6(1) (2016) 35863.

[11] J. Chen, Z. Yao, X. Wang, Y. Lu, X. Wang, Y. Liu, X. Fan, Effect of C content on microstructure and tensile properties of as-cast CoCrFeMnNi high entropy alloy, Materials Chemistry and Physics 210 (2018) 136-145.

[12] J. Kumar, A. Linda, M. Sadhasivam, K. Pradeep, N. Gurao, K. Biswas, The effect of Si addition on the structure and mechanical properties of equiatomic CoCrFeMnNi high entropy alloy by experiment and simulation, Materialia 27 (2023) 101707.

[13] W. Jiang, X. Gao, Y. Cao, Y. Liu, Q. Mao, L. Gu, Y. Zhao, Charpy impact behavior and deformation mechanisms of Cr26Mn20Fe20Co20Ni14 high-entropy alloy at ambient and cryogenic temperatures, Materials Science and Engineering: A 837 (2022) 142735.

[14] H. Chang, T. Zhang, S. Ma, D. Zhao, R. Xiong, T. Wang, Z. Li, Z. Wang, Novel Si-added CrCoNi medium entropy alloys achieving the breakthrough of strength-ductility trade-off, Materials & Design 197 (2021) 109202.

[15] D. Xu, M. Wang, T. Li, X. Wei, Y. Lu, A critical review of the mechanical properties of CoCrNi-based medium-entropy alloys, Microstructures 2(1) (2022) 2022001.

[16] B. Gludovatz, A. Hohenwarter, K.V. Thurston, H. Bei, Z. Wu, E.P. George, R.O. Ritchie, Exceptional damage-tolerance of a medium-entropy alloy CrCoNi at cryogenic temperatures, Nature communications 7(1) (2016) 10602.

[17] J. Miao, C. Slone, T. Smith, C. Niu, H. Bei, M. Ghazisaeidi, G. Pharr, M.J. Mills, The evolution of the deformation substructure in a Ni-Co-Cr equiatomic solid solution alloy, Acta Materialia 132 (2017) 35-48.

[18] D.B. Miracle, O.N. Senkov, A critical review of high entropy alloys and related concepts, Acta Materialia 122 (2017) 448-511.

[19] G. Laplanche, A. Kostka, C. Reinhart, J. Hunfeld, G. Eggeler, E. George, Reasons for the superior mechanical properties of medium-entropy CrCoNi compared to high-entropy CrMnFeCoNi, Acta Materialia 128 (2017) 292-303.

[20] Z. Li, L. Chen, P. Fu, H. Su, P. Dai, Q. Tang, The effect of Si addition on the heterogeneous grain structure and mechanical properties of CrCoNi medium entropy alloy, Materials Science and Engineering: A 852 (2022) 143655.

[21] J.B. Seol, J.W. Bae, Z. Li, J.C. Han, J.G. Kim, D. Raabe, H.S. Kim, Boron doped ultrastrong and ductile high-entropy alloys, Acta Materialia 151 (2018) 366-376.

[22] M. Klimova, D. Shaysultanov, A. Semenyuk, S. Zherebtsov, G. Salishchev, N. Stepanov, Effect of nitrogen on mechanical properties of CoCrFeMnNi high entropy alloy at room and cryogenic temperatures, Journal of alloys and compounds 849 (2020) 156633.

[23] D. Wei, L. Wang, Y. Zhang, W. Gong, T. Tsuru, I. Lobzenko, J. Jiang, S. Harjo, T. Kawasaki, J.W. Bae, Metalloid substitution elevates simultaneously the strength and ductility of face-centered-cubic high-entropy alloys, Acta Materialia 225 (2022) 117571.

[24] H. Yi, M. Bi, K. Yang, B. Zhang, Significant Improvement the mechanical properties of CoCrNi alloy by tailoring a dual FCC-phase structure, Materials 13(21) (2020) 4909.

[25] J.-J. Chen, P.-H. Chiu, T.-R. Chen, T.-C. Tsao, Y.-A. Chen, S.-Y. Lu, C.-Y. Tseng, C.-L. Tai, W.-S. Lee, R. Misra, Evolution of deformation structures in CrCoNiSi0. 3 medium entropy alloy subjected to high-strain-rate and quasi-static compressive deformation, Materials Characterization (2024) 114088.

[26] S.-W. Kim, J.H. Kim, In-situ observations of deformation twins and crack propagation in a CoCrFeNiMn high-entropy alloy, Materials Science and Engineering: A 718 (2018) 321-325.

[27] Z. Zhang, M. Mao, J. Wang, B. Gludovatz, Z. Zhang, S.X. Mao, E.P. George, Q. Yu, R.O. Ritchie, Nanoscale origins of the damage tolerance of the high-entropy alloy

CrMnFeCoNi, Nature communications 6(1) (2015) 10143.

[28] J. Liu, C. Chen, Y. Xu, S. Wu, G. Wang, H. Wang, Y. Fang, L. Meng, Deformation twinning behaviors of the low stacking fault energy high-entropy alloy: An in-situ TEM study, Scripta Materialia 137 (2017) 9-12.

[29] Y.-C. Hsieh, L. Zhang, T.-F. Chung, Y.-T. Tsai, J.-R. Yang, T. Ohmura, T. Suzuki, In-situ transmission electron microscopy investigation of the deformation behavior of spinodal nanostructured δ-ferrite in a duplex stainless steel, Scripta Materialia 125 (2016) 44-48.

[30] M.-Y. Gao, S.-P. Tsai, J.-R. Yang, Y.-L. Chang, T. Ohmura, C.-Y. Chen, S.-H. Wang, Y.-T. Wang, C.-Y. Huang, In-situ transmission electron microscopy investigation of compressive deformation in interphase-precipitated carbide-strengthened α-iron single-crystal nanopillars, Materials Science and Engineering: A 746 (2019) 406-415.

[31] D. Hull, D.J. Bacon, Introduction to dislocations, Elsevier2011.

[32] L. Huang, Q.-J. Li, Z.-W. Shan, J. Li, J. Sun, E. Ma, A new regime for mechanical annealing and strong sample-size strengthening in body centred cubic molybdenum, Nature communications 2(1) (2011) 547.

[33] D. Kiener, P. Hosemann, S.A. Maloy, A.M. Minor, In situ nanocompression testing of irradiated copper, Nature materials 10(8) (2011) 608-613.

[34] S. Bajpai, B.E. MacDonald, T.J. Rupert, H. Hahn, E.J. Lavernia, D. Apelian, Recent progress in the CoCrNi alloy system, Materialia (2022) 101476.